Investigation of Shifted Bit Dependent Error in Analog-to-Digital Converters

By
Eric William Swanson
B.S. University of Maine, 1996

A THESIS
Submitted in Partial Fulfillment of the
Requirements for the Degree of
Master of Science
(in Electrical Engineering)

The Graduate School
University of Maine
May 1998

Advisory Committee:

Fred H. Irons, Castle Professor of Electrical and Computer Engineering, Advisor

Donald M. Hummels, Associate Professor of Electrical and Computer Engineering

Allison I. Whitney, Lecturer in Electrical and Computer Engineering

Library Rights Statement

Investigation of Shifted Bit Dependent Error in Analog-to-Digital Converters

By Eric William Swanson

Thesis Advisor: Dr. Fred H. Irons

An Abstract of the Thesis Presented

in Partial Fulfillment of the Requirements for the

Degree of Master of Science

(in Electrical Engineering)

May 1998

As the popularity of electronic communications devices grows so does the demand for higher speed products. With an increase in the production of high speed parts comes changes in the limitations of these parts. The analog-to-digital converter (ADC) is an essential building block in many of today's high speed communication systems. As ADC's are operating at higher sampling frequencies the dominant error mechanisms in these converters are also changing.

This thesis investigates a dynamic error mechanism not identified in literature to date. In this thesis the mechanism is referred to as shifted-bit dependent error. The source of this error can be determined by calculating correlation coefficients between current error samples and previous bits of a converter output. This provides a "picture" of the ADC output error dependent upon previous output sample bits. This type of error, where current samples are affected by portions of previous output samples, is sometimes encountered as a second order error in

pipelined flash architectures and as a first order mechanism in the emerging high-speed folding architectures.

In addition to introducing methods to identify and quantify this error mechanism, this thesis proposes a digital correction scheme which can be used to improve the linearity of the converter. A calibration procedure is introduced which uses an orthogonal search technique to identify the set of dominant bits affecting the converter error. These error contributions may then be subtracted (digitally) from the converter output, improving the spurious free dynamic range (SFDR) of the converter. Results of this work are presented in this thesis for both simulated and experimental data. Improvements obtained in SFDR were about 20 dB for a simulated model, and as much as 10 dB for experimental data. These results have shown great promise for this method of ADC compensation for those devices that exhibit this type of repeatable error.

ACKNOWLEDGMENTS

This work has been supported in part by the ARPA Digital Receiver program under a contract administered by the Office of Naval Research Grant N66001-97-C-8617.

This work has also been supported in part by the Roger C. Castle fund which began in 1990.

I would like to extend special thanks to Roger C. Castle who has been a great financial support for me as well as a very dear friend. I would also like to say thank you to Fred H. Irons for noticing in my second year at the University of Maine that I have some scholarly potential, and for being much more than just my professor. Thank you, Donald M. Hummels for always having an answer to any question I ask. Thank you Allison Whitney for keeping me entertained with your great assortment of neckties. Thank you Leora M. Swanson and Paul G. Swanson for always standing behind me in all the choices I've made in my life. Thank you, Shelly for giving me a reason to succeed, and thank you Connie Riechel for telling me that I could.

TABLE OF CONTENTS

LIST OF FIGURES

CHAPTER 1

Introduction

As the applications and demand for higher speed analog-to-digital converters (ADCs) increases so does the demand for increased dynamic range. In order to meet these demands a great deal of effort has been put forth investigating architectural problems in many of today's popular ADC structures. As converter speed is pushed further into the GHz range new sources of distortion arise. Until the cause of these new distortions are found a "quick fix" is sometimes implemented. This "quick fix" is a compensation scheme where the dominant error mechanism in a converter is modelled using a set of basis functions. This thesis investigates a new technique for finding and modelling error which may be present in modern high-speed ADCs.

1.1 Background

Work in the field of ADC compensation has been active for several years. Much of this work however, has focused on modelling error [6] as a function of the state (ADC output code) and slope of the input signal [5, 8, 9]. The preferred method of modelling error has been a two dimensional functional approximation with state and slope used as independent variables. In this procedure a converter is driven with several sinusoid test trajectories and an error function is generated from which a table is created with state and slope values as the indices. When the table is accessed, an error value is selected and this quantity is subtracted from the current sample thus providing a compensated sample. This method has proven to be quite successful, but not perfect, at improving spurious free dynamic range (SFDR). This has led to research into different error mechanisms.

1.2 Purpose of This Research

Others have looked extensively at state and slope dependent error modelling. Past research has not however, accounted for all harmonic distortion introduced by many high-speed converters. With ADCs sampling at or above a GHz the dominant error mechanisms begin to change. There are significant errors remaining after state-slope errors are removed.

This work investigates a phenomena referred to as shifted-bit error. The principle behind shifted-bit error is that since, in many ADC topologies it takes several clock cycles for a signal to be digitized, the output bits could be feeding back into the board affecting a later output sample.

The purpose of this thesis is to develop a new diagnostic tool and error compensation scheme applicable to the shifted-bit dependent error mechanism. A technique of plotting correlation coefficients versus clock cycles of shift will be used to verify the existence of shifted-bit error. Then an orthogonal search technique is developed to identify a dominant set of basis bits and their coefficients to compensate for this type of error.

1.3 Thesis Organization

This thesis introduces the idea of shifted-bit dependent error in ADCs. All procedures necessary to detect, model and compensate for these errors are introduced.

Chapter 2 introduces a method of detecting shifted-bit dependent errors. This detection procedure is based upon a technique of correlating the harmonic errors of an ADC with shifted output bits. This procedure uses the standard definition of correlation coefficients with a slight twist added to accommodate multiple calibration data sets into the model. Chapter 3 describes a method of error modeling based on the classic least squares solution. Such a solution is found using a technique called the Slow Orthogonal Search (SOS). The development of the SOS technique is discussed in detail. At the end of Chapter 3 a shifted-bit error compensation routine is outlined. Chapter 4 contains the results of concepts derived in both Chapters 2 and 3 for both theoretical (simulated) and real ADC data. Results include plots of SFDR, effective number of bits (ENOB), and Spectral plots. Finally, Chapter 5 presents conclusions drawn from the research performed for this thesis.

CHAPTER 2

Error Detection

As the demand upon ADCs to perform at higher speed and resolution continues to grow, research has turned to looking at what are the limitations of today's converters. For example, much work has been done in looking at the harmonic error in an ADC as a function of the output code and the slope of the input signal [8, 9, 3, 10]. State and slope error modeling has proven to provide great improvement in the spurious-free dynamic range (SFDR) while not sacrificing the effective number of bits (ENOB). State and slope error models have not however, identified all sources of harmonic distortion introduced by a non-ideal quantizer. For this reason it may be convenient to provide a way of investigating other error sources. This chapter develops a new error detection tool to evaluate ADC error dependence upon previous, or shifted, bits out of an ADC.

2.1 ADC Error as a Function of Previous (Shifted) Output Bits

Error introduced into a quantized sample which is a function of its binary representation is known as "digital kickback". In many of today's ADC's the conversion process takes several clock cycles to be completed. It is therefore reasonable to assume that errors could be strongly correlated to either the binary representation of previous samples or bit transitions in those representations. For example, if an ADC needs five clock cycles to output its four-bit output code, it's logical that the idea of digital kickback is applicable here. Any or all of the four bits at the output of the converter could feedback to input comparators or the track/hold circuitry. In this case, error introduced into the input sample may be a function of any of the four output bits from a sample taken five clock cycles earlier. Consequently it is useful to derive a method of relating previous bit values to the harmonic distortion in an output code.

2.1.1 Relating Previous Bits to Error in the Output Code

Trying to relate previous bit values to errors in an output code requires a definition of the error to model. The first step is to define quantities relative to the ADC output: let $x(t)$ be the time domain input into the ADC. The i^{th} ADC output sample may then be written in terms of $x(t)$ as shown in (2.1).

$$y_i = x(i \cdot T_s) + e_i \tag{2.1}$$

In this expression T_s is the sample period, and e_i is the unknown error of the i^{th} sample. Next let y_i have binary representation given in (2.2) where N_b is the number of output bits.

$$(b_{i,1}, b_{i,2}, \cdots, b_{i,N_b}) \tag{2.2}$$

The goal is to predict e_i based on previous values of these bits. The desired relationship between past bits and error values is displayed in (2.3).

$$\hat{e}_i = \sum_{n=0}^{N_{sh}} \sum_{j=1}^{N_b} \theta_{n,j} \cdot b_{i-n,j} \tag{2.3}$$

A quick indication of important bits in the above approximation may be obtained by examining the ability to predict e_i using a single previous bit $b_{i-n,j}$.

Equation (2.4) is the error estimate based on a single previous bit, and (2.5) is the optimal choice for θ.

$$\hat{e}_i = \theta \cdot b_{i-n,j} \tag{2.4}$$

$$\theta = \frac{E\{e_i \cdot b_{i-n,j}\}}{E\{b_{i-n,j}^2\}} \tag{2.5}$$

The mean-square error associated with this estimate can be written in terms of the correlation coefficient as in (2.6).

$$E\{(e_i - \hat{e}_i)^2\} = E\{e_i^2\} \cdot (1 - \rho^2) \tag{2.6}$$

The correlation coefficient ρ is defined for the n^{th} delay and j^{th} bit as in (2.7).

$$\rho_{n,j} = \frac{E\{e_i \cdot b_{i-n,j}\}}{E\{e_i^2\}^{\frac{1}{2}} \cdot E\{b_{i-n,j}^2\}^{\frac{1}{2}}} \tag{2.7}$$

The i^{th} bit is important (small mean-square error) if the magnitude of ρ is close to 1 and is unimportant if the magnitude of ρ is close to 0. This same reasoning can be extended to include several samples. For this it is convenient to introduce a matrix notation.

Now, let $\vec{y}$ be an N element vector of ADC output samples as displayed in (2.8).

$$\vec{y} = \vec{x} + \vec{e} \tag{2.8}$$

In this expression for $\vec{y}$, $\vec{x}$ is the sampled input signal and $\vec{e}$ is the vector of error to model. A binary matrix $\tilde{B}_n$ can also be defined which has its i^{th} row given by the binary representation of the delayed sample y_{i-n}. This matrix is given in (2.9).

$$\tilde{B}_n = \begin{bmatrix} b_{1-n,1} & b_{1-n,2} & \dots & b_{1-n,N_b} \\ b_{2-n,1} & b_{2-n,2} & \dots & b_{2-n,N_b} \\ \vdots & \vdots & \ddots & \vdots \\ b_{1,1} & b_{1,2} & \dots & b_{1,N_b} \\ \vdots & \vdots & \ddots & \vdots \\ b_{N-n,1} & b_{N-n,2} & \dots & b_{N-n,N_b} \end{bmatrix} \tag{2.9}$$

With the introduction of this notation (2.3) can be rewritten in a condensed notation as in (2.10).

$$\hat{\vec{e}} = \sum_{n=0}^{N_{sh}} \tilde{B}_n \cdot \vec{\alpha}_n = \tilde{H} \cdot \vec{\alpha} \tag{2.10}$$

In the above expression $\tilde{H}$ is defined to be the matrix made up of all the desired shift matrices B_n for $n = 0, 1, \cdots, N_{sh} - 1$ as shown in (2.11), where N_{sh} is the desired number of shifts to investigate.

$$\tilde{H} = [\tilde{B}_0 \tilde{B}_1 \cdots \tilde{B}_{N_{sh}-1}] \tag{2.11}$$

When the error, $\vec{e}$, is linearly dependent upon previous bit values of the converter, then it should be correlated to some columns of the matrices $\tilde{B}_0$ through $\tilde{B}_{N_{sh}-1}$. For example, if the error in a sample is due entirely to the most significant bit (MSB) of the output code from the fifth previous sample then $\vec{e}$ exhibits a perfect linear dependence upon the first column of $\tilde{B}_5$. To find which previous bit values are most correlated to the error in a graphical manner, the correlation coefficient between the error and each bit of the converter at N_{sh} different shifts can be calculated and plotted.

2.1.2 Estimating The Shifted Bit Correlation Coefficient

By calculating a correlation coefficient between the error and previous bit values a plot showing where the error originated can be produced.

The method of calculating the correlation coefficients is shown in (2.12) through (2.17). In these equations N is the total number of samples collected, and $\tilde{B}_0(i,j)$ is the $(i,j)^{th}$ element in the shifted-bit matrix, $\tilde{B}_0$.

$$M_e = \frac{1}{N} \cdot \sum_{i=1}^{N} e_i \tag{2.12}$$

$$M_B(j) = \frac{1}{N} \cdot \sum_{i=1}^{N} \tilde{B}_0(i,j) \tag{2.13}$$

$$\sigma_e{}^2 = \left(\frac{1}{N} \cdot \sum_{i=1}^{N} e_i^2\right) - M_e^2 \tag{2.14}$$

$$\sigma_B{}^2(j) = \left(\frac{1}{N} \cdot \sum_{i=1}^{N} \tilde{B}_0^2(i,j)\right) - M_B^2 \tag{2.15}$$

$$C_{eB_n}(j) = \left(\frac{1}{N} \cdot \sum_{i=1}^{N} e_i \cdot \tilde{B}_n(i,j)\right) - M_e \cdot M_B(j) \tag{2.16}$$

$$r_{eB_n}(j) = \left|\frac{C_{eB_n}(j)}{\sigma_e \cdot \sigma_B(j)}\right| \tag{2.17}$$

$$\text{Where: } j = 1, 2, ..., N_b$$

$$n = 0, 1, ..., N_{sh} - 1$$

In (2.12) through (2.17), M_e is the sample mean of the error and $M_B(j)$ is the mean for each bit, where j is the bit (1,2,...,N_b). σ_e^2 and $\sigma_B^2(j)$ are variances of the error and binary outputs respectively. Finally, $C_{eB_n}(j)$ is the covariance of the error with each of the bits (j) at the shift values (n). The resulting correlation coefficient magnitudes, $r_{eB_n}(j)$, relate the MSB through LSB at a particular shift value (n) to the error of the converter.

In practice, the converter error $\vec{e}$ cannot be directly measured. For high speed devices, the input signal $x(t)$ cannot be controlled with precision adequate to directly calculate the error terms e_i. To circumvent this problem, the converter may be calibrated by driving the input with a filtered sinusoidal signal with an integer number of cycles over the data collection period. By using sinusoidal calibration signals, several practical difficulties with the above procedures can be addressed. First, the periodic nature of the calibration signal implies that negative delay times associated with the first n rows of B_n may be replaced by samples taken from the end of the sample buffers. Secondly (and more important), the above expressions for e_i and the columns of $\tilde{B}_n$ may be replaced by the corresponding signals extracted from the harmonics of the input signal frequency [5]. This procedure avoids the difficulty of estimating the actual error e_i, while retaining the majority of the energy in the error waveforms. Fast Fourier transforms (FFT's) may be used to extract the desired harmonics from y_i and $b_{i,j}$.

The sinusoidal structure of $x(t)$ has an unwanted effect of artificially introducing a periodicity in the correlation with delayed bits. To avoid obtaining periodicity in the correlation coefficients due to using sinusoidal test signals, the coefficients, r_{eB_n}, must be calculated using several independent test frequencies. The selection of signal amplitude must also be considered. The amplitudes of trajectories used to calculate r_{eBn} must span the entire working range of the converter or, they must all drive the converter near full loading. Using several trajectories requires updating the correlation coefficient parameters for each of N_T sample sets. The update equations are shown in (2.18) through (2.23).

$$
\begin{aligned}
M_e^{TOT} &= \frac{1}{N \cdot N_T} \cdot \sum_{i=1}^{N} \left(e_i^{(1)} + e_i^{(2)} + \cdots + e_i^{(N_T)}\right) && (2.18)\\
M_B^{TOT}(j) &= \frac{1}{N \cdot N_T} \cdot \sum_{i=1}^{N} \left(\tilde{B}_0^{(1)}(i,j) + \tilde{B}_0^{(2)}(i,j) + \cdots + \tilde{B}_0^{(N_T)}(i,j)\right) && (2.19)\\
\sigma_e^{TOT2} &= \frac{1}{N \cdot N_T} \cdot \sum_{i=1}^{N} \left({e_i^{(1)}}^2 + {e_i^{(2)}}^2 + \cdots + {e_i^{(N_T)}}^2\right) - M_e^{TOT2} && (2.20)\\
\sigma_B^{TOT2}(j) &= \frac{1}{N \cdot N_T} \cdot \sum_{i=1}^{N} ({\tilde{B}_0^{(1)}}^2(i,j) + {\tilde{B}_0^{(2)}}^2(i,j) + \cdots \\
&\qquad + {\tilde{B}_0^{(N_T)}}^2(i,j)) - M_B^{TOT2} && (2.21)\\
C_{eB_n}^{TOT}(j) &= \frac{1}{N \cdot N_T} \cdot \sum_{i=1}^{N} (e_i^{(1)} \cdot \tilde{B}_n^{(1)}(i,j) + e_i^{(2)} \cdot \tilde{B}_n^{(2)}(i,j) + \cdots \\
&\qquad + e_i^{(N_T)} \cdot \tilde{B}_n^{(N_T)}(i,j)) - M_e^{TOT} \cdot M_B^{TOT}(j) && (2.22)\\
r_{eB_n}^{TOT}(j) &= \left| \frac{C_{eB_n}^{TOT}(j)}{\sigma_e \cdot \sigma_B(j)} \right| && (2.23)\\
\text{Where: } j &= 1, 2, ..., N_b \\
n &= 0, 1, ..., N_{sh} - 1
\end{aligned}
$$

These quantities can be accumulated for several desired shift values (0,1,...,$N_{sh}-1$) and frequencies (N_T), and a plot showing the magnitude correlation of error to previous bit values can be generated.

2.2 Shifted Bit Correlation Plot Example

Returning to the example where the error in a four bit converter is solely dependent upon the MSB from the fifth previous output sample, a plot of the magnitude of correlation coefficient versus shifted-bit value can be generated using the above analysis method. Figure 2.1 shows the resulting plot. Since the error of the quantizer is modelled to depend solely upon the MSB of the fifth previous clock

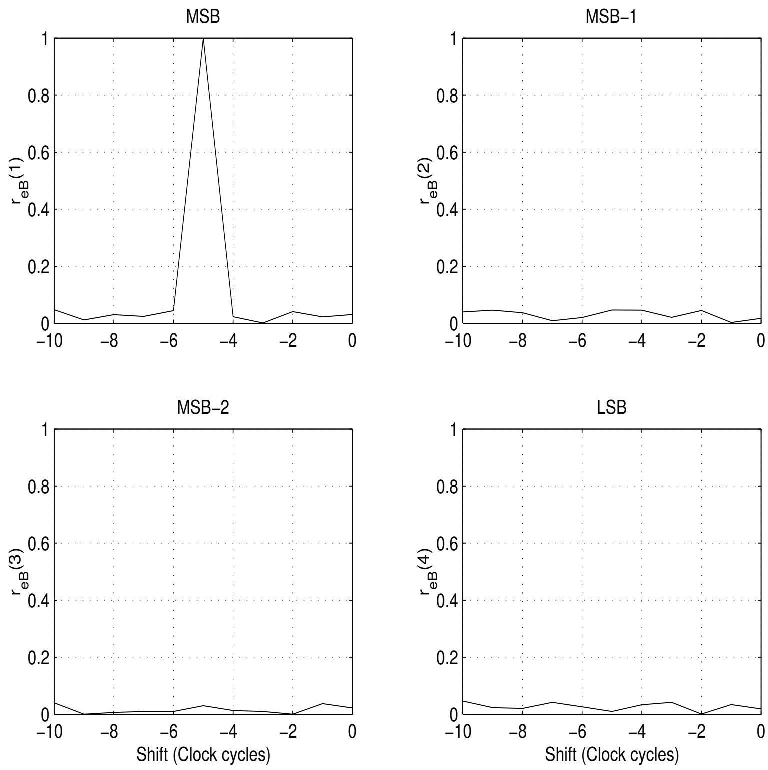

Figure 2.1: Correlation plot of shifted-bits and harmonic distortion, theoretical error model

cycle, the correlation magnitude at this point is exactly one. If the error were also dependent upon another shifted-bit value, or any of many other potential error sources (state, slope, previous state of the converter) this coefficient would have been smaller in magnitude. A correlation coefficient can vary over the range -1 to +1. A correlation coefficient of 1 demonstrates a strong linear relationship, -1 signifies a strong inverse dependence, and 0 signifies no dependence. For this reason, the magnitude of the coefficient is important, not its sign.

2.3 Shifted Bit Correlation Plot Summary

This section outlines all the necessary steps required to produce a shifted-bit correlation plot. The plotting routine's summary is as follows.

1. Collect several N-sample trajectories of data from an ADC by driving it independently with several sinewaves each at better than 1/2 of the ADC's fullscale voltage and varying frequencies.

2. Calculate $\tilde{B}_0$ through $\tilde{B}_{N_{sh}-1}$ for every trajectory.

3. Calculate the fast fourier transform, (FFT), of each trajectory, also calculate the FFT of $\tilde{B}_0$ through $\tilde{B}_{N_{sh}-1}$ for every trajectory.

4. Generate $\vec{e}$ by selecting a set of harmonic components from the FFT of the samples for each trajectory and calculate the inverse fast fourier transform (IFFT) for this set. Do the same for each of the $\tilde{B}_n$ matrices of each trajectory, i.e., replace $\tilde{B}_n$ with the IFFT of the desired harmonic components of the original $\tilde{B}_n$.

5. Calculate the N_b correlation coefficients between $\vec{e}$ and the selected harmonic components of $\tilde{B}_n$ for $n = 0, 1, ..., N_{sh}-1$ updating the summations as shown in (2.18) through (2.23).

6. Plot the correlation coefficient magnitude versus shift value for every bit (MSB to LSB).

CHAPTER 3

ADC Error Modelling

Now that a technique has been formulated for detecting shifted-bit errors the next logical step is to derive a method of bit dependent error extraction. The correlation plots determine if there is a linear dependence of the error on shifted-bit values, but it doesn't suggest how the error can be removed. This chapter looks into finding the best linear solution for shifted-bit dependent error. The traditional method of modeling data is with a least squares fit. To begin Chapter 3 the least squares fit to shifted-bit dependent error is formulated.

3.1 The Least Squares Solution

A least squares solution for $\vec{e}$ would require writing it as a linear combination of the columns of $\tilde{H}$ as shown in (3.1). Thus there are $N_b \cdot N_{sh}$ possible unknown coefficients labeled θ_j, $j = 1, 2, \cdots, N_b \cdot N_{sh}$.

$$\hat{\vec{e}}_i = \sum_{j=1}^{N_b \cdot N_{sh}} \theta_j \cdot H_{i,j} = \tilde{H} \cdot \vec{\theta} \tag{3.1}$$

Equation (3.2) shows the $\tilde{H}$ matrix in terms of the shifted-bit matrices defined in (2.9).

$$\tilde{H} = [\tilde{B}_0, \tilde{B}_1, ..., \tilde{B}_{N_{sh}-1}] \tag{3.2}$$

$\vec{\theta}$ is a column vector of $N_b \cdot N_{sh}$ coefficients which weights the columns of $\tilde{H}$ to describe $\vec{e}$. Since it is quite impractical to think that $\vec{e}$ could be perfectly described by $\tilde{H}\cdot\vec{\theta}$ it is customary to assume there will be some error in the estimate. Let $\vec{\epsilon}$ denote the error in the estimate, $\vec{\epsilon} = \vec{e} - \hat{\vec{e}}$, giving (3.3).

$$\vec{e} = \tilde{H} \cdot \vec{\theta} + \vec{\epsilon} \tag{3.3}$$

The goal of the least squares solution is to minimize the squared error term $\vec{\epsilon}^T \cdot \vec{\epsilon}$. The solution for $\vec{\theta}$ which minimizes this squared error given by [12], and is shown in (3.4).

$$\vec{\theta} = (\tilde{H}^T \cdot \tilde{H})^{-1} \cdot \tilde{H}^T \cdot \vec{e} \tag{3.4}$$

This is the classical least squares solution for the k^{th} trajectory but in this formulation it has a few shortcomings. In preparation of avoiding the problem this solution has, three new quantities are introduced: $\tilde{G}$,$\vec{r}$, and E which are the Gram matrix, correlation vector, and sum squared error respectively.

$$\tilde{G} = \tilde{H}^T \cdot \tilde{H} \tag{3.5}$$

$$\vec{r} = \tilde{H}^T \cdot \vec{e} \tag{3.6}$$

$$E = \vec{e}^T \cdot \vec{e} \tag{3.7}$$

With these expressions defined it is easy to see that $\vec{\theta}$ can be written in terms of the Gram matrix and the correlation vector.

$$\vec{\theta} = \tilde{G}^{-1} \cdot \vec{r} \tag{3.8}$$

This section has presented the solution for basis coefficients, $\vec{\theta}$, for a single trajectory. When several trajectories are incorporated together the solution quickly becomes impractical.

3.2 A Limitation of the Least Squares Solution

For this work the classical least squares solution is impractical since for a single sinusoid trajectory there is a strong periodicity in the correlation coefficients. To eliminate this periodicity this technique needs to be fitted to several trajectories of data. In fact, each time a new trajectory is encountered $\tilde{H}$ must be updated as in (3.9).

$$\tilde{H}_{new} = \begin{bmatrix} \tilde{H}_{old} \\ \tilde{H}^{(k)} \end{bmatrix} \tag{3.9}$$

$\tilde{H}$ quickly grows too large to be handled by even today's computing power! For example, a typical trajectory may have 16384 samples, it may come from an 8-bit converter, and when tested at 10 shift values for 30 trajectories $\tilde{H}$ grows to a dimension of 491520×80. With dimensions this large the least squares solution quickly becomes impossible to compute. Because of this limitation a new, memory managing, technique must be implemented. The next two sections introduces techniques to overcome this memory problem.

3.3 Combining Multiple Calibration Measurements

Multiple calibration measurements must be taken to reduce periodic tendencies in the correlation vector, $\vec{r}$, which make the solution for $\vec{\theta}$ incorrect. Adding trajectories changes (3.3) to the following.

$$
\begin{bmatrix} \vec{e}^{(1)} \\ \vec{e}^{(2)} \\ \vdots \\ \vec{e}^{(N_T)} \end{bmatrix} = \begin{bmatrix} \tilde{H}^{(1)} \\ \tilde{H}^{(2)} \\ \vdots \\ \tilde{H}^{(N_T)} \end{bmatrix} \cdot \vec{\theta} + \vec{\epsilon} \tag{3.10}
$$

Where N_T is the number of trajectories

In this case $\tilde{H}$ is now too large to store. However, $\tilde{H}$ doesn't need to be stored to calculate $\vec{\theta}$ if a method of updating $\tilde{G}$, $\vec{r}$, and E can be found. Starting with the expression for $\vec{\theta}$ given in (3.4) we have (3.11).

$$
\hat{\vec{\theta}} = (\tilde{H}^T \cdot \tilde{H})^{-1} \cdot \tilde{H}^T \cdot \vec{e} \tag{3.11}
$$

where $\tilde{H}$, and $\vec{e}$ are redefined as in (3.10). This expression leads to changes in the Gram matrix, correlation vector, and the sum squared error to accomodate several test trajectories as follows.

$$
\tilde{G} = \tilde{H}^T \cdot \tilde{H} = \sum_{k=1}^{N_T} \tilde{H}^{(k)^T} \cdot \tilde{H}^{(k)} = \sum_{k=1}^{N_T} \tilde{G}^{(k)} \tag{3.12}
$$

$$
\vec{r} = \tilde{H}^T \cdot \vec{e} = \sum_{k=1}^{N_T} \tilde{H}^{(k)^T} \cdot \vec{e}^{(k)} = \sum_{k=1}^{N_T} \vec{r}^{(k)} \tag{3.13}
$$

$$
E = \vec{e}^T \cdot \vec{e} = \sum_{k=1}^{N_T} \vec{e}^{(k)^T} \cdot \vec{e}^{(k)} = \sum_{k=1}^{N_T} E^{(k)} \tag{3.14}
$$

In the above expressions $\tilde{G}^{(k)}$, $\vec{r}^{(k)}$, and $E^{(k)}$ are the Gram matrix, the correlation vector, and the sum squared error of the k^{th} trajectory respectively.

When implementing this procedure it is much easier to maintain running totals of $\tilde{G}$, $\vec{r}$, and E than to save $\tilde{H}$ since the sizes of these quantities never change. With each new trajectory these quantities can be updated as follows,

$$\tilde{G}_{new} = \tilde{G}_{old} + \tilde{G}^{(k)} \tag{3.15}$$

$$\vec{r}_{new} = \vec{r}_{old} + \vec{r}^{(k)} \tag{3.16}$$

$$E_{new} = E_{old} + E^{(k)} \tag{3.17}$$

where "old" designates the results including all trajectories before the k^{th} and "new" signifies the result after the k^{th} trajectory is included. Once $\tilde{G}$, $\vec{r}$, and E have been updated to include each trajectory the coefficients, $\vec{\theta}$, can then be calculated using (3.8). However, if most of these coefficients are essentially zero it is better to only calculate significant coefficients. A method of finding "significant" coefficients is presented in the following section.

3.4 The Slow Orthogonal Search (SOS)

The slow orthogonal search is a searching routine based on the same fundamental concepts as the fast orthogonal search (FOS) [1, 2, 7]. When trying to fit data to a set of potential basis vectors (the columns of $\tilde{H}$), an orthogonal search algorithm will search through the set of candidate basis vectors and select the vector which minimizes the sum squared error in the estimate. After a selection is made, the routine will then eliminate any linear dependence of that vector from the remaining set of candidate basis vectors before making the next selection.

The goal of this routine is to efficiently minimize $\vec{\epsilon}^T \cdot \vec{\epsilon}$ to form the best linear fit to the ADC error. In so doing a relationship between the selected basis vector (a column of $\tilde{H}$) and the elements of $\tilde{G}$, $\vec{r}$, and E must be developed. With a little manipulation of (3.3) it is easy to obtain (3.18).

$$\vec{\epsilon}^T \cdot \vec{\epsilon} = \vec{e}^T \cdot \vec{e} - \vec{e}^T \cdot \tilde{H} \cdot (\tilde{H}^T \cdot \tilde{H})^{-1} \cdot \tilde{H}^T \cdot \vec{e} \tag{3.18}$$

The effect of selecting the m^{th} column of $\tilde{H}$ as a new basis vector is obtained by replacing $\tilde{H}$ by the selected column of $\tilde{H}$. The resulting sum squared error is given by (3.19).

$$\vec{\epsilon}^T \cdot \vec{\epsilon} \approx \vec{e}^T \cdot \vec{e} - \vec{e}^T \cdot \vec{h}_m \cdot (\vec{h}_m^T \cdot \vec{h}_m)^{-1} \cdot \vec{h}_m^T \cdot \vec{e} \tag{3.19}$$

The goal is to identify the value of m which reduces the sum-squared error the most. That is, find the index, m, of the column of $\tilde{H}$ which is most linearly related to the error vector $\vec{e}$. This index value is the desired quantity from this manipulation and by finding this index value the desired most sensitive column of $\tilde{H}$ is also found.

To find m it is crucial to look at this minimization more closely. To minimize the sum squared error ($\vec{\epsilon}^T \cdot \vec{\epsilon}$) it is easy to see that the quantity after the minus sign in (3.19) must be maximized. This quantity and its equivalence in terms of $\tilde{G}$, and $\vec{r}$ is displayed in (3.20).

$$\vec{e}^T \cdot \vec{h}_m \cdot (\vec{h}_m^T \cdot \vec{h}_m)^{-1} \cdot \vec{h}_m^T \cdot \vec{e} = \frac{r_m^2}{G_{m,m}} \tag{3.20}$$

From (3.20) it is clear that m is the index of the maximum of the division of the elements of $\vec{r}$ by the corresponding diagonal elements of $\tilde{G}$. Once the "best" index is found, the search continues until the desired number of columns has been selected.

3.4.1 Updating $\tilde{G}$,$\vec{r}$,E After Each Column Selection

Since the routine is designed to be an "orthogonal" search every time a column of $\tilde{H}$ is selected, the remaining columns must be made independent of the selected column. This ensures the next selection is not biased by a strong linear relation to the previous. To make the remaining columns of $\tilde{H}$ independent from the chosen column, $\vec{h}_m$, the *projection matrix* $\tilde{P}_m$ [12] is calculated as shown.

$$\tilde{P}_m = \vec{h}_m \cdot (\vec{h}_m^T \cdot \vec{h}_m)^{-1} \cdot \vec{h}_m^T \tag{3.21}$$

The matrix $(\tilde{I} - \tilde{P}_m)$ may be used to find the component of any vector, $\vec{x}$, which is orthogonal to $\vec{h}_m$. This quantity could be applied to $\vec{e}$ and $\tilde{H}$ to make the remaining columns of $\tilde{H}$ independent to the m^{th} column of $\tilde{H}$ as in equations (3.22) and (3.23).

$$\tilde{H}' = (\tilde{I} - \tilde{P}_m) \cdot \tilde{H} \tag{3.22}$$

$$\vec{e}\,' = (\tilde{I} - \tilde{P}_m) \cdot \vec{e} \tag{3.23}$$

However, $\tilde{H}$ is not explicitly stored, so we need to examine how the above change in $\tilde{H}$ modifies $\tilde{G}$,$\vec{r}$,and E. In (3.24) through (3.26) the projection matrix is applied to $\tilde{G}$, $\vec{r}$, and E to create $\tilde{G}'$, $\vec{r}\,'$, and E' after the m^{th} column is selected.

$$\begin{aligned} \tilde{G}' &= \tilde{H}'^T \cdot \tilde{H}' \\ &= \tilde{H}^T \cdot (\tilde{I} - \tilde{P}_m) \cdot (\tilde{I} - \tilde{P}_m) \cdot \tilde{H} \\ &= \tilde{H}^T \cdot \tilde{H} - \tilde{H}^T \cdot \vec{h}_m \cdot (\vec{h}_m^T \cdot \vec{h}_m)^{-1} \cdot \vec{h}_m^T \cdot \tilde{H} \end{aligned} \tag{3.24}$$

$$
\begin{aligned}
\vec{r}\,' &= \tilde{H}' \cdot \vec{e}' \\
&= \tilde{H}^T \cdot (\tilde{I} - \tilde{P}_m) \cdot (\tilde{I} - \tilde{P}_m) \cdot \vec{e} \\
&= \tilde{H}^T \cdot \vec{e} - \tilde{H}^T \cdot \vec{h}_m \cdot (\vec{h}_m^T \cdot \vec{h}_m)^{-1} \cdot \vec{h}_m^T \cdot \vec{e}
\end{aligned} \tag{3.25}
$$

$$
\begin{aligned}
E' &= \vec{e}\,'^T \cdot \vec{e}\,' \\
&= \vec{e}\,' \cdot (\tilde{I} - \tilde{P}_m) \cdot (\tilde{I} - \tilde{P}_m) \cdot \vec{e} \\
&= \vec{e}^T \cdot \vec{e} - \vec{e}^T \cdot \vec{h}_m \cdot (\vec{h}_m^T \cdot \vec{h}_m)^{-1} \cdot \vec{h}_m^T \cdot \vec{e}
\end{aligned} \tag{3.26}
$$

The results displayed in (3.24) through (3.26) can now be rewritten in terms of the columns and elements in $\tilde{G}$ and $\vec{r}$. Equations (3.27) through (3.29) show how to update equations for $\tilde{G}$,$\vec{r}$, and E after each basis function selection.

$$\tilde{G}' = \tilde{G} - \frac{\vec{g}_m \cdot \vec{g}_m^T}{G_{m,m}} \tag{3.27}$$

$$\vec{r}\,' = \vec{r} - \frac{\vec{g}_m \cdot r_m}{G_{m,m}} \tag{3.28}$$

$$E' = E - \frac{r_m^2}{G_{m,m}} \tag{3.29}$$

In (3.27) through (3.29), $\vec{g}_m$ is the m^{th} column of $\tilde{G}$, $G_{m,m}$ is the m^{th} diagonal element in $\tilde{G}$ and r_m is the m^{th} element in $\vec{r}$.

With this new set of equations independent from the selected column, the search continues for another column until E' reaches some threshold value, or the desired number of columns has been chosen. With this procedure complete the final step in the routine is to calculate the basis function coefficients, $\hat{\vec{\theta}}$.

3.4.2 Estimating the Basis Function Coefficients

Estimating the basis function coefficients is easy once the desired number of basis functions have been selected. Equation (3.8) calculates a coefficient for every column of $\tilde{H}$ but it is more practical to find coefficients for just the columns selected in the orthogonal search. To do this, the information in $\tilde{G}$ and $\vec{r}$ corresponding to the selected columns of $\tilde{H}$ must be extracted.

A simpler notation is obtained for the selected set of basis coefficients by defining $\tilde{G}_M$ and $\vec{r}_M$ as the Gram matrix and correlation vector for the selected basis set.

$$\tilde{G}_M = \begin{bmatrix} G_{m_1,m_1} & G_{m_1,m_2} & \cdots & G_{m_1,m_{N_{sel}}} \\ G_{m_2,m_1} & G_{m_2,m_2} & \cdots & G_{m_2,m_{N_{sel}}} \\ \vdots & \vdots & \ddots & \vdots \\ G_{m_{N_{sel}},m_1} & G_{m_{N_{sel}},m_2} & \cdots & G_{m_{N_{sel}},m_{N_{sel}}} \end{bmatrix} \tag{3.30}$$

$$\vec{r}_M = \begin{bmatrix} r_{m_1} \\ r_{m_2} \\ \vdots \\ r_{m_{N_{sel}}} \end{bmatrix} \tag{3.31}$$

In the above expressions $m_i =$ the i^{th} selection. With $\tilde{G}_M$ and $\vec{r}_M$ defined, the solution for the desired number of basis coefficients simplifies to the solution shown in (3.32) for $\vec{\theta}_M$.

$$\vec{\theta}_M = \tilde{G}_M^{-1} \cdot \vec{r}_M \tag{3.32}$$

The calibration routine is completed with the basis coefficients thus determined. These coefficients and their corresponding indices, can be used to compensate for shifted-bit dependent errors in the ADC. The next section presents a summary of the shifted-bit error calibration procedure.

3.5 Calibration Algorithm Summary

The steps which follow are a summary of the neccesary steps to calculate basis function coefficients for a shifted-bit dependent error model.

1. Collect a large set of trajectories from the ADC at varying frequencies and several, near full scale, amplitudes.

2. Extract relevant harmonics from the FFT of the samples to generate $\vec{e}$. Extract the same harmonic components from the shifted-bit matrices to generate $\tilde{H}$.

3. Calculate the Gram matrix $\tilde{G}$, the correlation vector $\vec{r}$, and the sum squared error term E as shown in (3.5), (3.6), and (3.7) for the first trajectory.

4. Update $\tilde{G}$,$\vec{r}$, and E using (3.15) through (3.17) for all additional test trajectories.

5. Find the first "best fit" column index using (3.20).

6. Update $\tilde{G}$,$\vec{r}$, and E using (3.27) through (3.29) and then find the next best fit column by repeating (3.20).

7. Continue the procedure until the desired number of columns have been selected or a specified error threshold is met.

8. Calculate $\vec{\theta}_M$ using (3.32).

When the coefficients have been calculated according to the above procedure calibration is complete. The next step is to apply the error model in a correction scheme. The next section reviews the entire compensation process.

3.6 Compensation Summary

Two important vectors are returned from the calibration routine. The first is the vector of coefficients, $\vec{\theta}_M$, and the second, denoted $\vec{M}$, is the vector of corresponding indices into the columns of $\tilde{H}$. Since this is a linear model, application of compensation is straightforward and is detailed in the following set of steps.

1. Collect a vector of samples, $\vec{y}$, from a single test trajectory.

2. Calculate a corresponding shifted-bit matrix, $\tilde{H}_y$, as in (3.2).

3. Create a smaller $\tilde{H}_y$ matrix denoted $\tilde{H}_s$ from the basis function indices in $\vec{M}$ as shown in (3.33).

$$\tilde{H}_s = [\vec{h}_{m_1}, \vec{h}_{m_2}, ..., \vec{h}_{m_{N_{sel}}}] \tag{3.33}$$

4. Calculate $\vec{e}_y$ as in (3.34) to estimate the error in the particular test trajectory.

$$\vec{e}_y = \tilde{H}_s \cdot \vec{\theta}_M \tag{3.34}$$

5. Subtract the estimated error from the sample set, $\vec{y}$, to obtain the compensated sample set, $\vec{y}_c$ as in (3.35).

$$\vec{y}_c = \vec{y} - \vec{e}_y \tag{3.35}$$

The vector $\vec{y}_c$ is the compensated data from the calibration procedure. The shifted-bit dependent error in this vector should be at a minimum. With the discussion of shifted-bit error modeling now complete, the next chapter presents results obtained using a simulated ADC as well as data from an actual converter.

CHAPTER 4

Results

The previous two chapters have developed techniques for detecting and modelling shifted-bit dependent error. Chapter 3 concludes by explaining how compensation of this type of error is achieved. This chapter presents results obtained for this research for both simulated and experimental ADC data.

4.1 ADC Simulation Results

As a first-cut experiment to test both concepts and software, a simulated converter with shifted-bit dependent error was created. The simulation modelled an 8-bit converter sampled at 204.8 MHz and tested over it's entire first Nyquist band. This ideal quantizer incorporated only two types of error,namely: dithered quantization error [11, 4], and shifted-bit dependent error. The bit dependent error was made up of four prior bits as follows:

- the MSB$-$2 bit from 9 clock cycles prior,
- the MSB$-$3 bit from 5 clock cycles prior,
- the MSB$-$4 bit from 9 clock cycles prior, and
- the MSB$-$5 bit from 5 clock cycles prior.

Every time one of these prior bits has a value of 1 then one-half of an LSB of error is added into the current sample before it is quantized. As much as 2 LSBs of error may therefore be added into a sample. As will be shown this error model creates a large amount of harmonic distortion. The next section shows bit correlation plots for data acquired from this simulated ADC model.

4.1.1 Shifted-Bit Correlation Plots

Using the above converter model the next step is to calculate correlation coefficients for each of the 8-bits of the converter over a set of N_{sh} shifts. The correlation coefficient plots in Figure 4.1 show correlation coefficient magnitudes for each of the 8-bits of the converter versus clock shift values (0,-1,...,-10). This plot was generated using 50 test trajectories (5 amplitudes, and 10 frequencies) and with 16384 samples collected for each trajectory (sample set). There are clearly four dominant and two minor "spikes" in this plot. The first, at a shift value of -9 clock cycles, represents the error in the current sample being linearly related to the MSB-2 bit from nine clock cycles prior. Similarly, the error has a linear dependence upon the MSB-3, MSB-4, and the MSB-5 from 5,9, and 5 prior clock cycles respectively. These are exactly as expected from the simulated converter's model except for the presence of the two minor spikes located at shifts of -5 and -9 in the MSB. These minor spikes at shifts of -5 and -9 exist since the input trajectories are sinusoidal. There is a strong negative correlation between the MSB and each of the lower order bits in the converter regardless of the trajectory amplitude (the larger the amplitude the less the correlation however). This correlation is due to the fact that similar harmonic components of these bits are used in the correlation process. These minor spikes will never be falsely chosen by the SOS if many of the input trajectories are larger than one half full scale loading. Now that the error has been detected the calibration procedes and compensation is performed.

4.1.2 Removal of Previous Bit Dependent Errors

As shown previously, the correlation plots identify bit dependent errors and a separate procedure is introduced to estimate that error. Chapter 3 lists

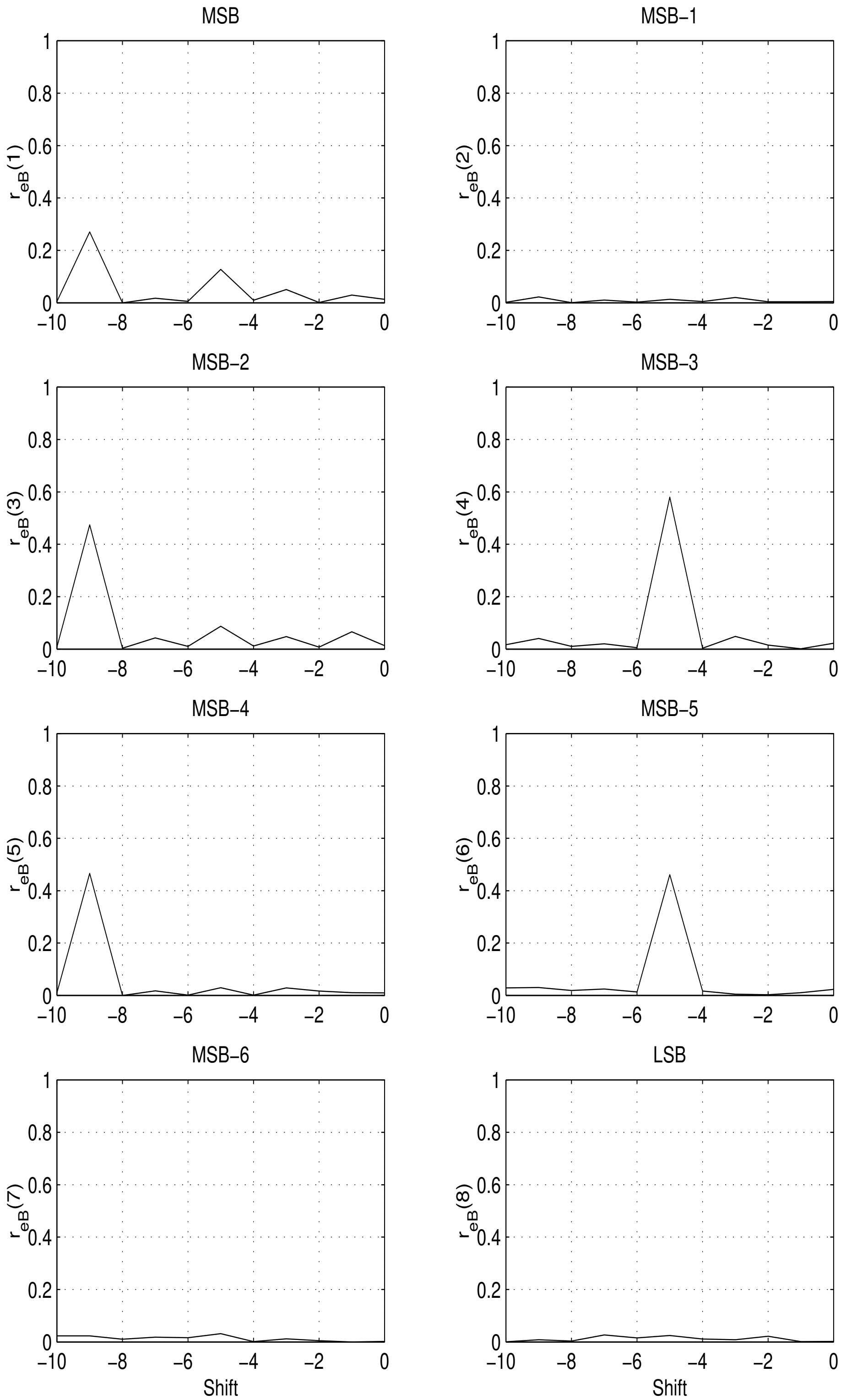

Figure 4.1: Correlation plot of shifted-bits and harmonic distortion, theoretical error model

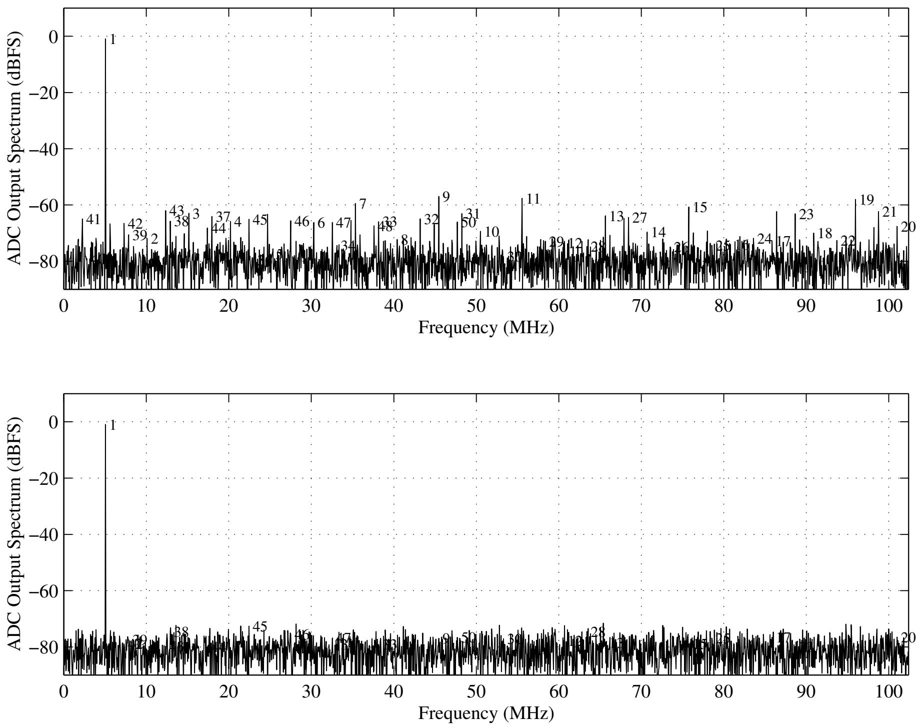

Figure 4.2: Uncompensated and compensated magnitude spectra, simulated results for a low frequency

all the necessary steps for calibrating and then compensating for this error. In implementing these procedures on the simulated converter from above, 5 basis coefficients were selected using the SOS routine. Test signal frequencies ranged from 2.5 to 100 MHz and amplitudes from 25 to 95 percent loading. Figures 4.2 through 4.4 show uncompensated and compensated magnitude FFT spectra for this 8-bit ADC model. These plots illustrate results obtained for test frequencies at the lower, middle, and upper frequencies of the first Nyquist band. The results clearly demonstrate that shifted-bit dependent error appears as rich, high order harmonic distortion across the full Nyquist band.

The compensation models the error perfectly for all three cases improving the simulated converter's SFDR over the entire band. Figure 4.5 compares the

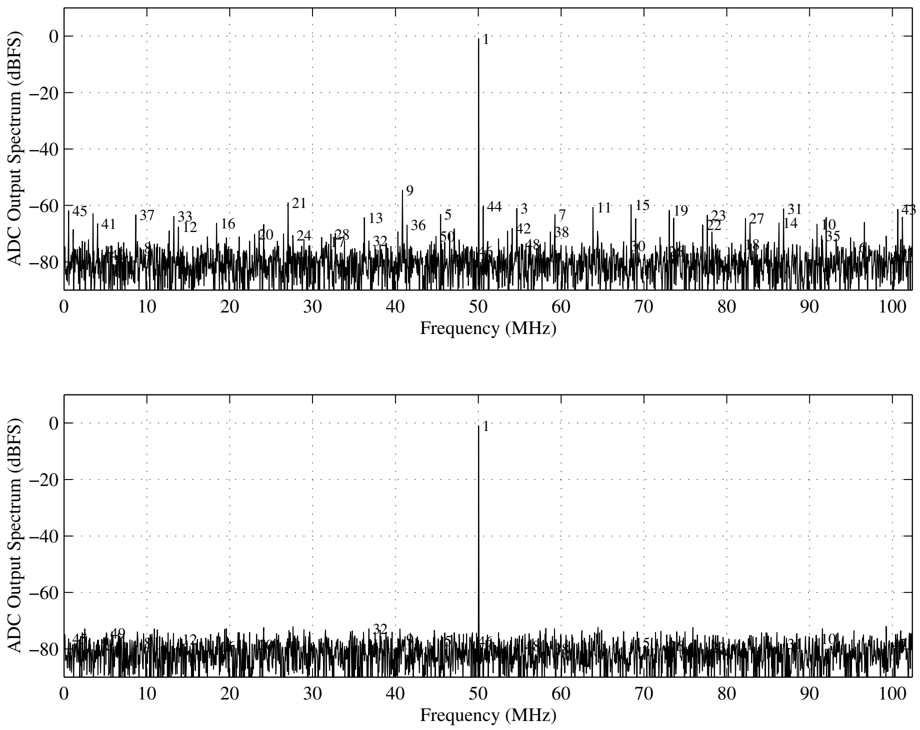

Figure 4.3: Uncompensated and compensated magnitude spectra, simulated results for a mid-Nyquist frequency

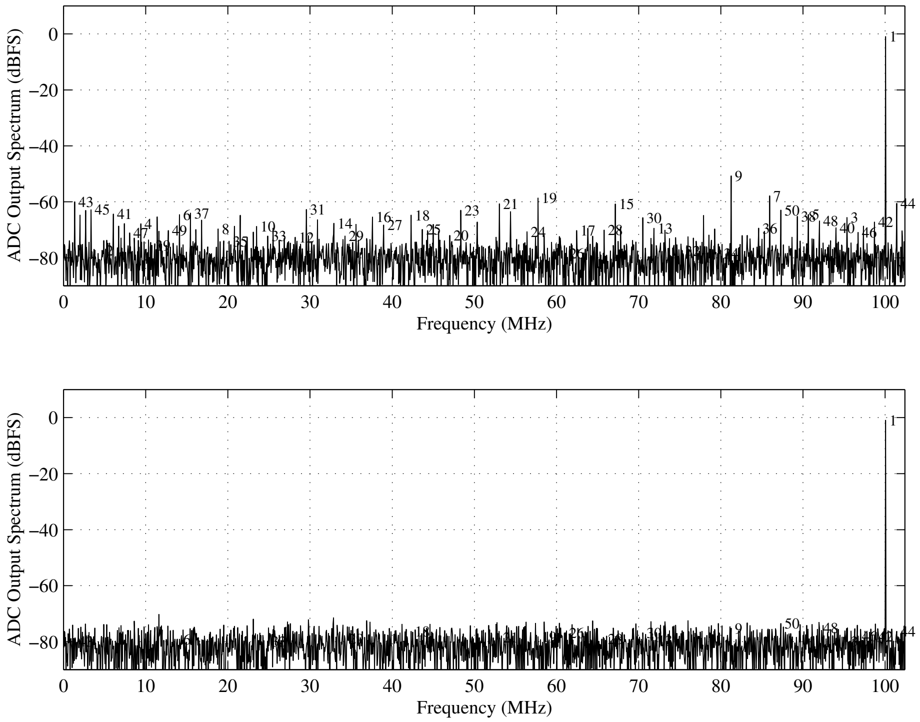

Figure 4.4: Uncompensated and compensated magnitude spectra, simulated results for a near-Nyquist frequency

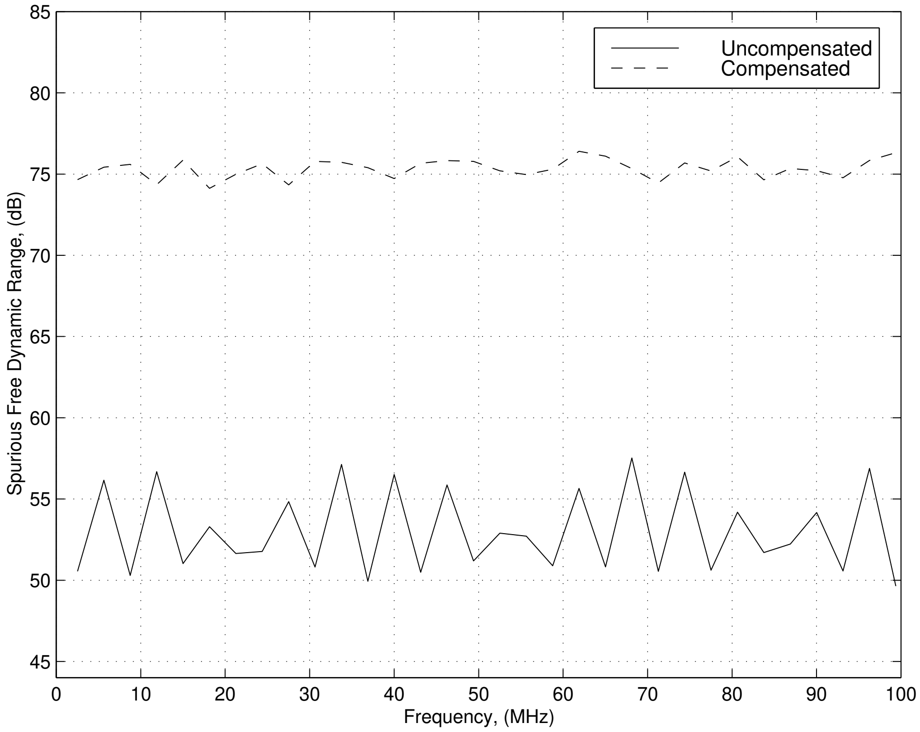

Figure 4.5: SFDR plot, simulated results

SFDR of the compensated and uncompensated data versus frequency over the entire first Nyquist band. SFDR is a measure of available dynamic range being a measure of the difference (in dB) of the fundamental harmonic and the next largest harmonic component,or spurious signal component in the magnitude spectra, ignoring the DC term.

For this simulation, the correction is broad band, working equally well across the full Nyquist band. The correction obtained is limited by the noise floor of the quantizer and the signal processing gain.

Another popular measurement in ADC characterization is the effective number of bits (ENOB). This measurement relates the power in the error to the quantization power of an ideal converter. It is referred to as ENOB since it is a figure

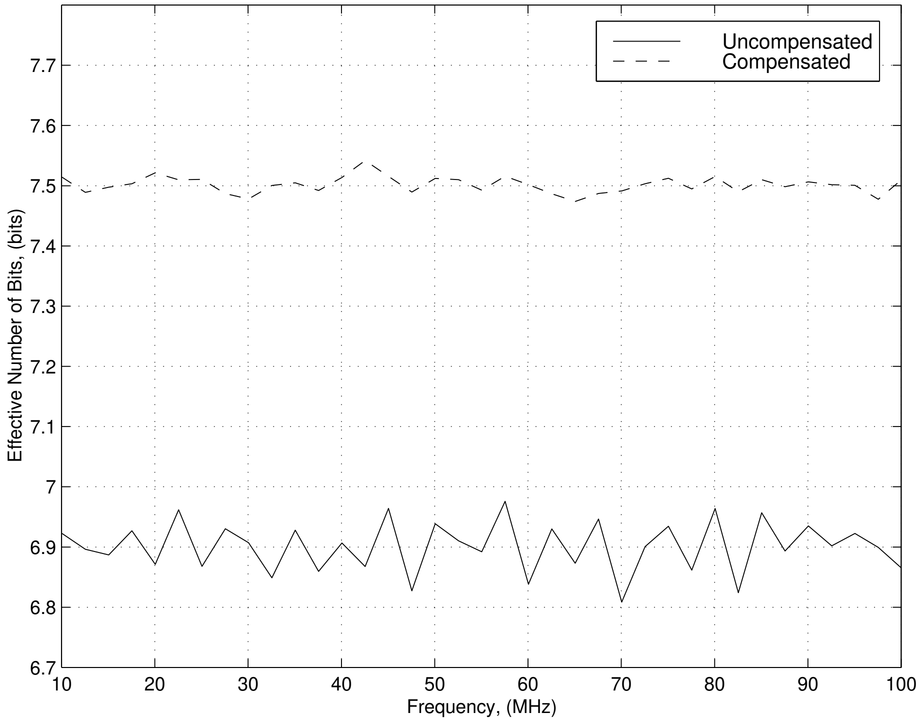

Figure 4.6: Effective number of bits over the first Nyquist band, simulated data

which determines the actual amount of information contained in the quantization process. Figure 4.6 shows that, for the simulated converter, no effective bits are lost in the compensating process; in fact, there is half a bit of improvement. This improvement is good because when compensation is performed there is the potential for SFDR improvement while introducing many new low-level harmonics to the input thereby possibly lowering the ENOB.

After compensation has been completed the shifted-bit dependent error should no longer exist. For this reason, correlation plots created using the compensated data no longer have the "spikes" which dominated the uncompensated data. A correlation plot for the post-compensation theoretical converter is shown in Figure 4.7. The result consists mostly of variations due to averaging out periodic error effects and does not exhibit the clear correlations obtained for uncompensated data especially when compared on the same plotting scale.

The simulation has shown, very clearly, the ability to detect and remove bit-dependent error from a source that contains such error.

4.1.3 Isolation of Shifted-Bit Error Mechanisms

To ensure that bit dependent error mechanisms are independent of state and slope models that have been previously researched, another ADC model is created using the same error mechanism of the previous section in addition to adding some state and slope dependent error. This state and slope dependent error is added in as second and third order functions of state and slope respectively. The state and slope dependent error is: $\frac{x^2}{5\cdot10^2} + \frac{y^3}{10^3}$ where x is state and y is slope. The first test performed on this converter is the creation of a shifted-bit correlation plot to show that state and slope error do not appear as zero shift error (digital kickback). Judging from Figure 4.8 and seeing no "spike" at zero shift for any of the bits, this is indeed the case with results nearly identical to those presented in Figure 4.1.

Next, the SOS technique was used to compensate out all bit dependent error. Figure 4.9 shows the only remaining distortions are the state dependent second and slope dependent third harmonics. The SOS technique appears to distinguish between bit dependent and non-bit dependent errors.

4.2 ADC Experimental Results

This section looks at experimental data obtained from a prototype 8-bit, 3 GHz ADC. This converter is sampled at 2.8 gigahertz and tested over its second Nyquist band. The error in this converter is potentially more diverse than

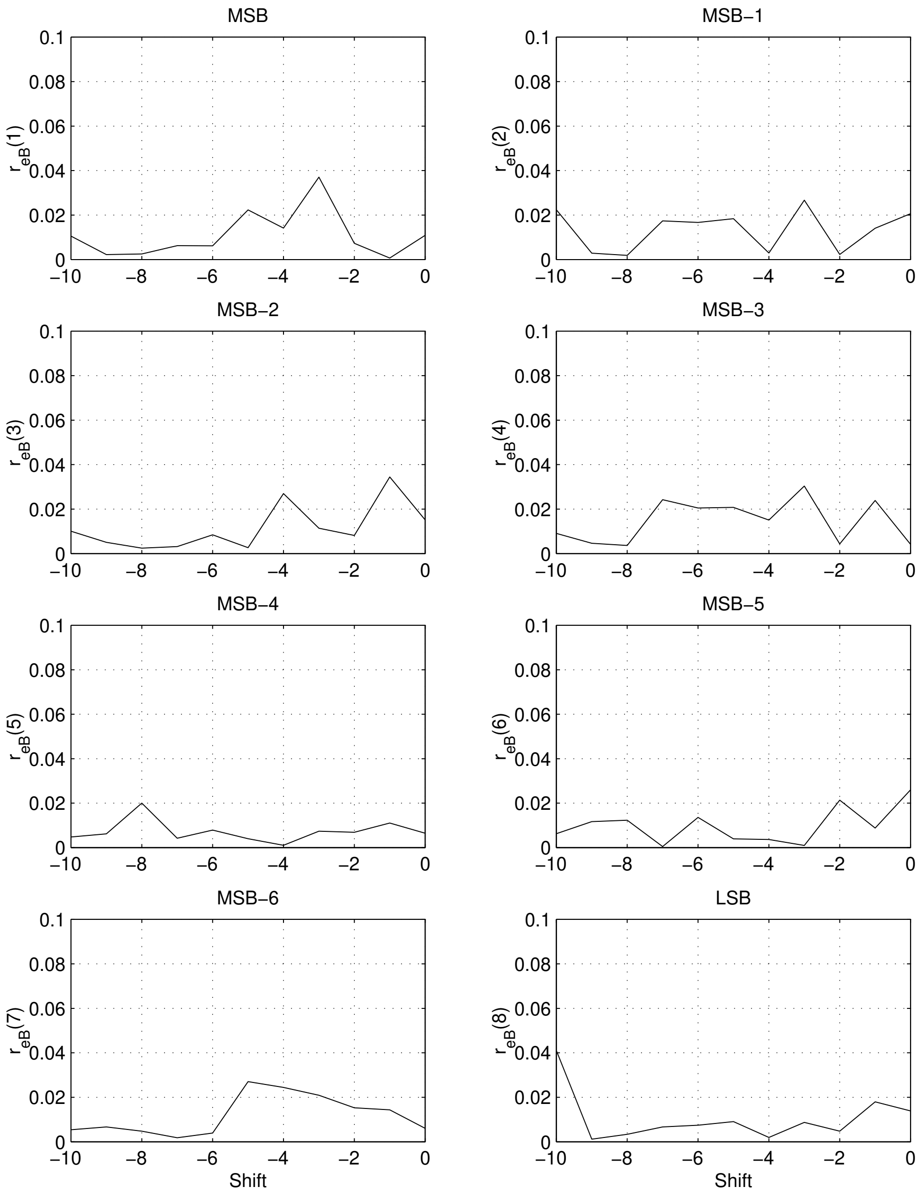

Figure 4.7: Correlation plot after compensation has been performed, simulated data

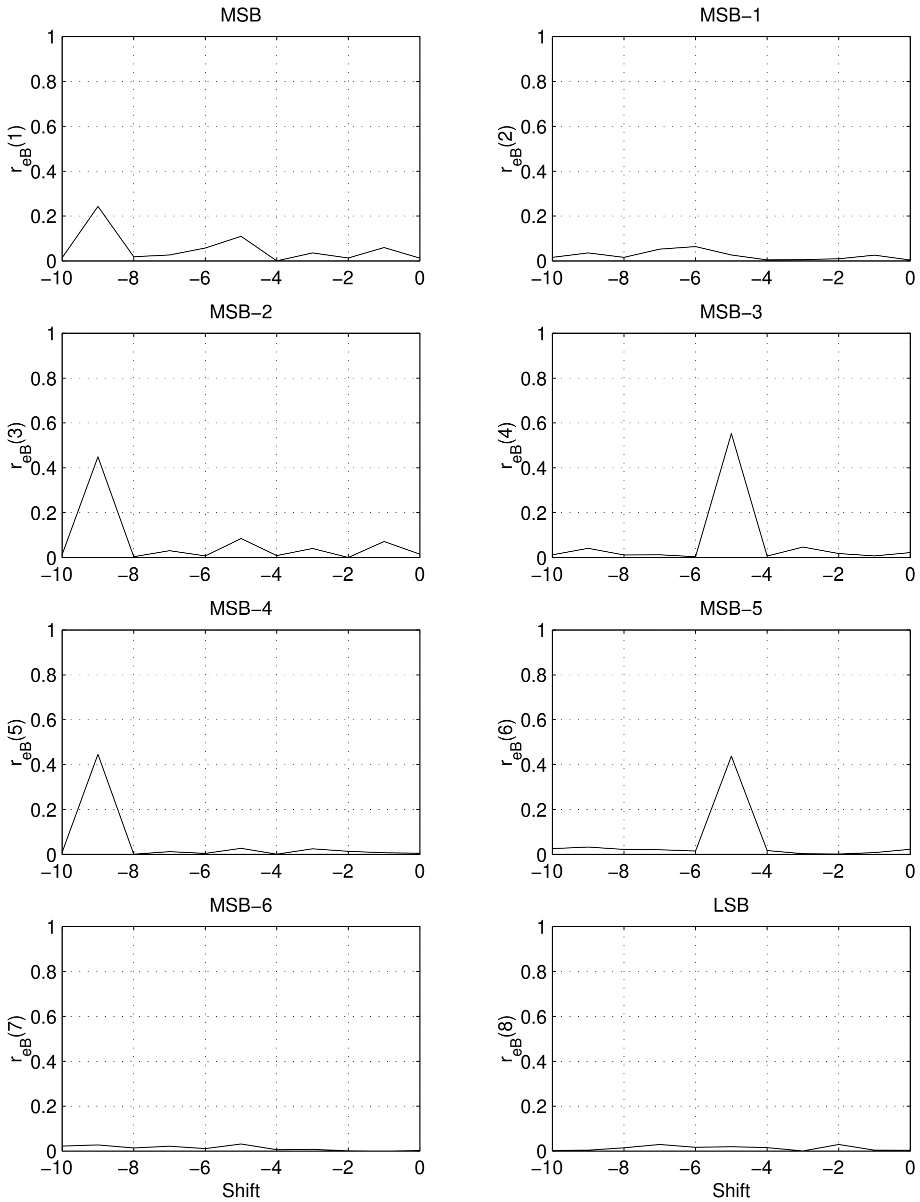

Figure 4.8: Correlation plot with state and slope dependent error included, simulated data

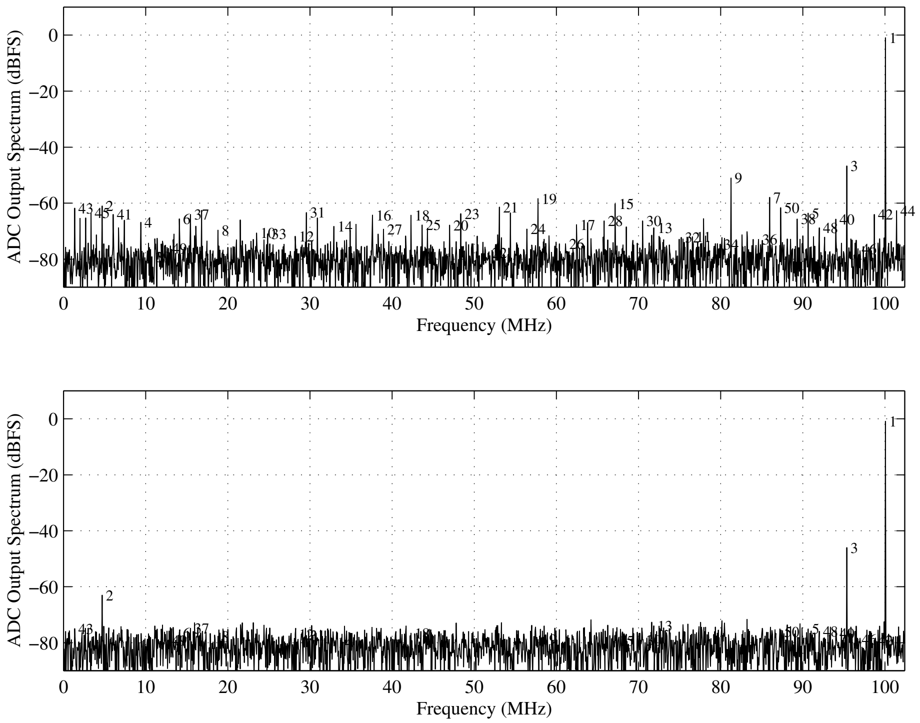

Figure 4.9: Uncompensated and compensated magnitude spectra with state and slope dependent error included, simulated data

the simulated converter in that shifted-bit errors are probably not the only source of harmonic distortion. However, with a high sampling frequency, shifted-bit dependent errors are more likely due to cross-talk between the output bits and the different stages of the quantization process on the board. This is illustrated in the next section.

4.2.1 Shifted-Bit Correlation Plots

The correlation plot shown in Figure 4.10 is for the 8-bit, 3 GHz prototype using 30 test trajectories. Test signal frequencies ranged from 1.4 to 2.8 GHz and amplitudes from 75 to 85 percent loading. There is a linear dependence of the error upon the first three MSBs, at zero shift. As explained in the introduction this is a form of digital kickback error. The calibration process is used to obtain a model for this error and compensation is applied in the next section.

4.2.2 Removal of Digital Kickback Error

Figures 4.11 through 4.13 show uncompensated and compensated magnitude spectra for the experimental converter. These plots cover the lower, middle, and upper frequencies of the *second* Nyquist band. As with the simulated converter there is a lot of harmonic distortion, but not all due to digital kickback. In Figure 4.11 the third harmonic dominates the spectrum in the uncompensated data, but is reduced by almost 10 dB when compensated. The mid-band plot, Figure 4.12, is not compensated as well. In fact, many harmonics look worse. The fifth harmonic is lowered but the third is virtually unaffected. In the mid-band of this converter this error is no longer dominated by the digital kickback error. In the upper half of the band the compensation begins to perform as well as it did

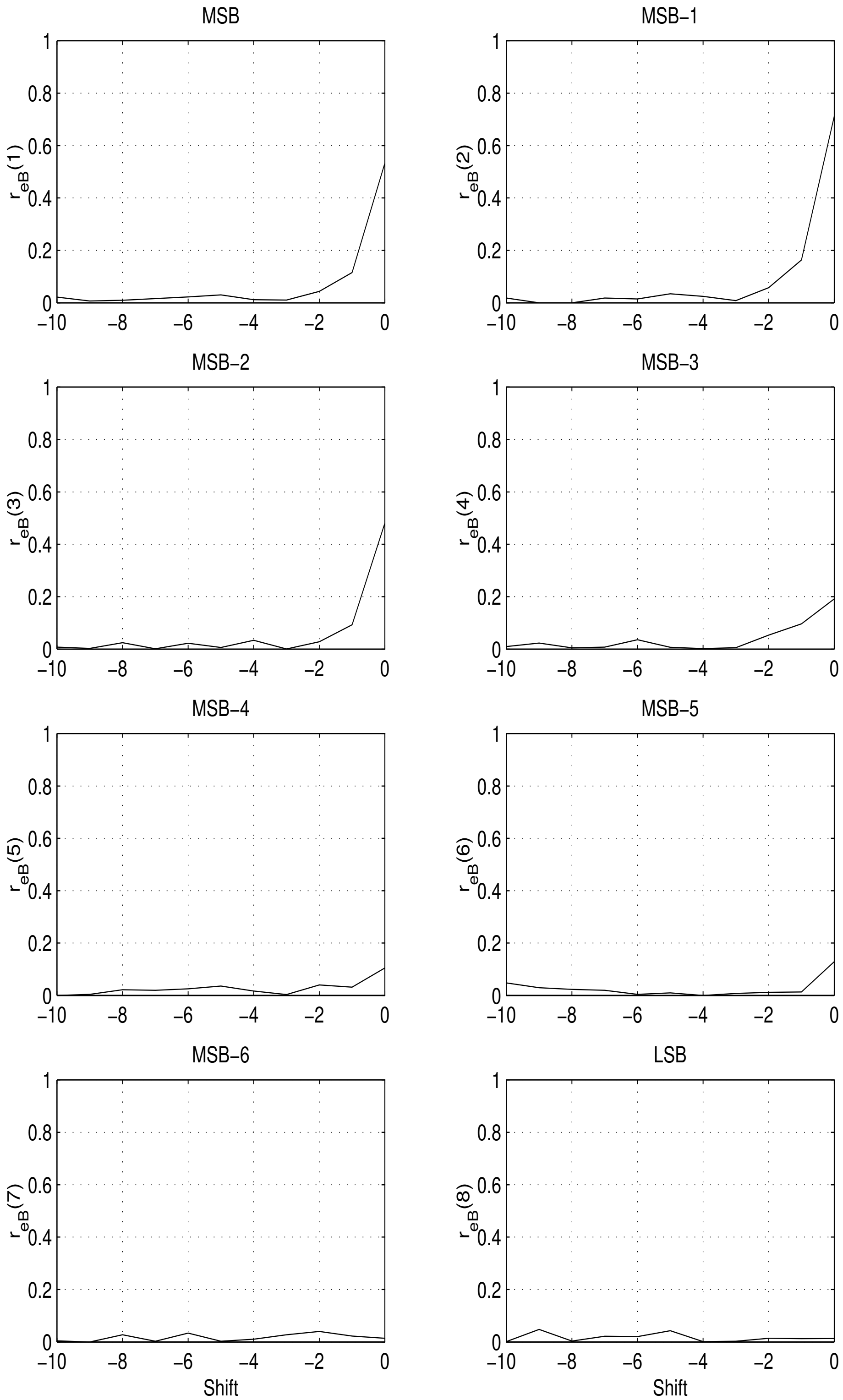

Figure 4.10: Correlation plot of shifted-bits and harmonic distortion, experimental data

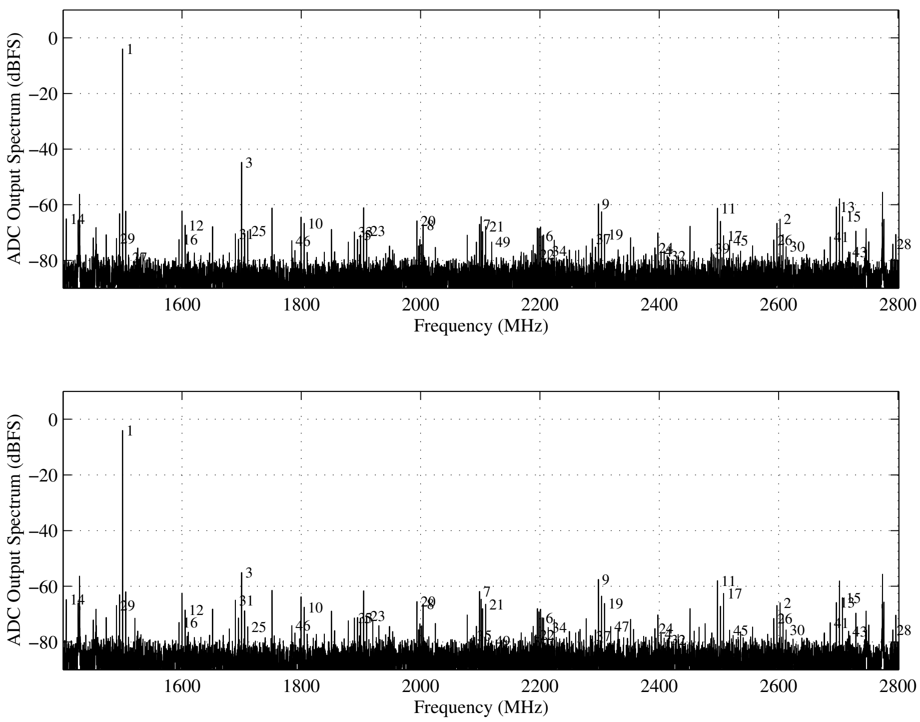

Figure 4.11: Uncompensated and compensated magnitude spectra, experimental results for a low frequency

for low frequencies, and is shown in Figure 4.13.

Figure 4.14 shows the SFDR for both compensated and uncompensated data. The lower and upper frequencies are compensated by as much as 10 dB, however, the mid-band frequencies are essentially unimproved. Figure 4.15 is a plot of the ENOB which shows that over most of the test frequencies the ENOB is improved nearly half a bit as was the case for the simulated ADC. The region which is slightly worse is due to over-compensation in this band of frequencies. Over-compensation is discussed further in Chapter 5.

Figure 4.16 shows the post-compensation correlation plot. It is easy to see that the coefficients are about an order of magnitude smaller than the originals shown in Figure 4.10.

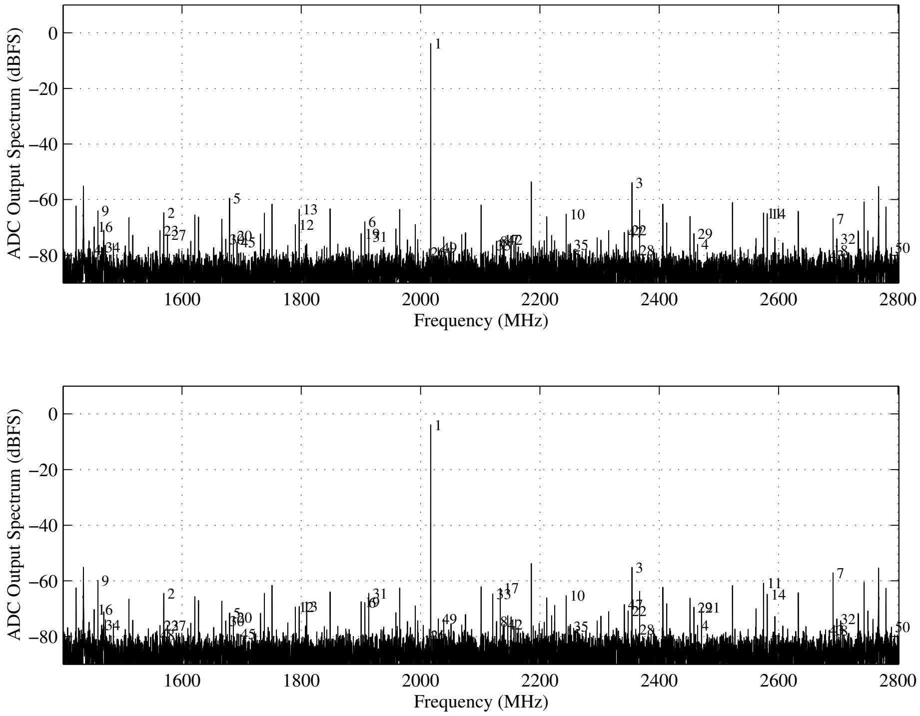

Figure 4.12: Uncompensated and compensated magnitude spectra, experimental results for a mid-Nyquist frequency

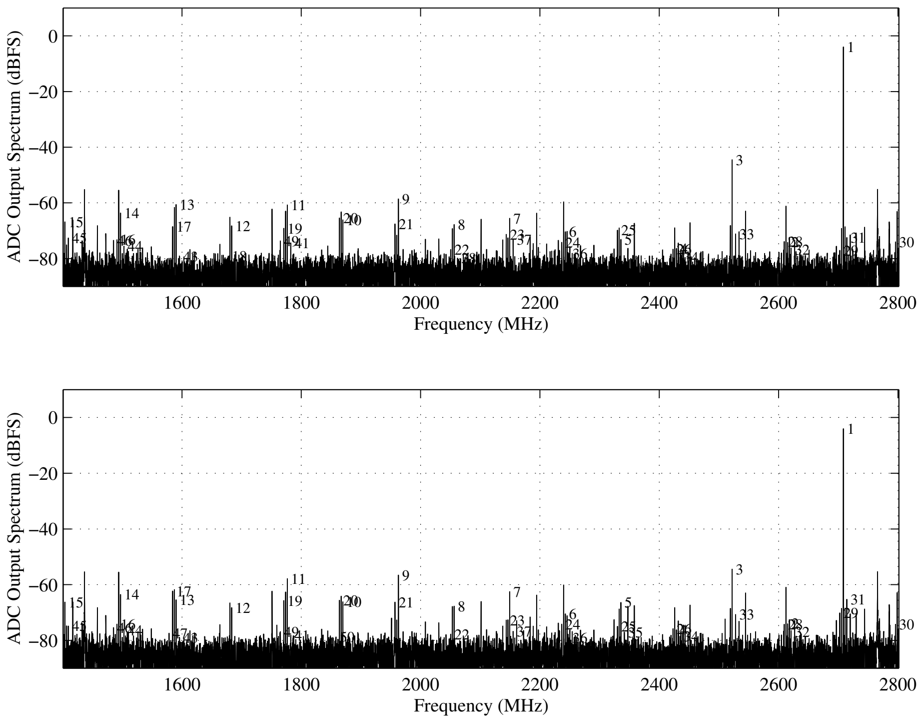

Figure 4.13: Uncompensated and compensated magnitude spectra, experimental results for a near-Nyquist frequency

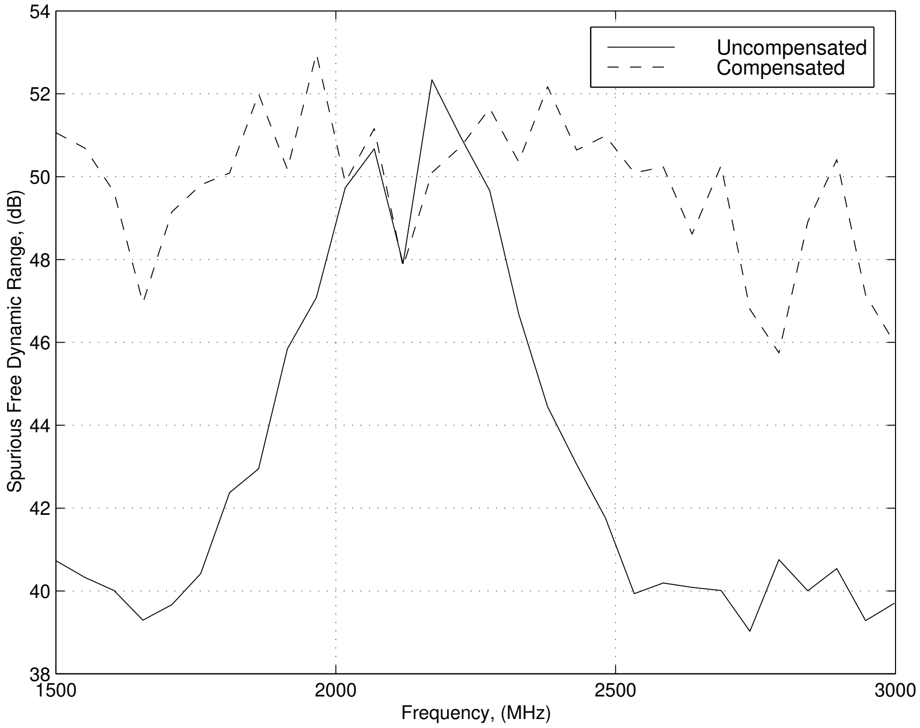

Figure 4.14: SFDR plot, experimental results

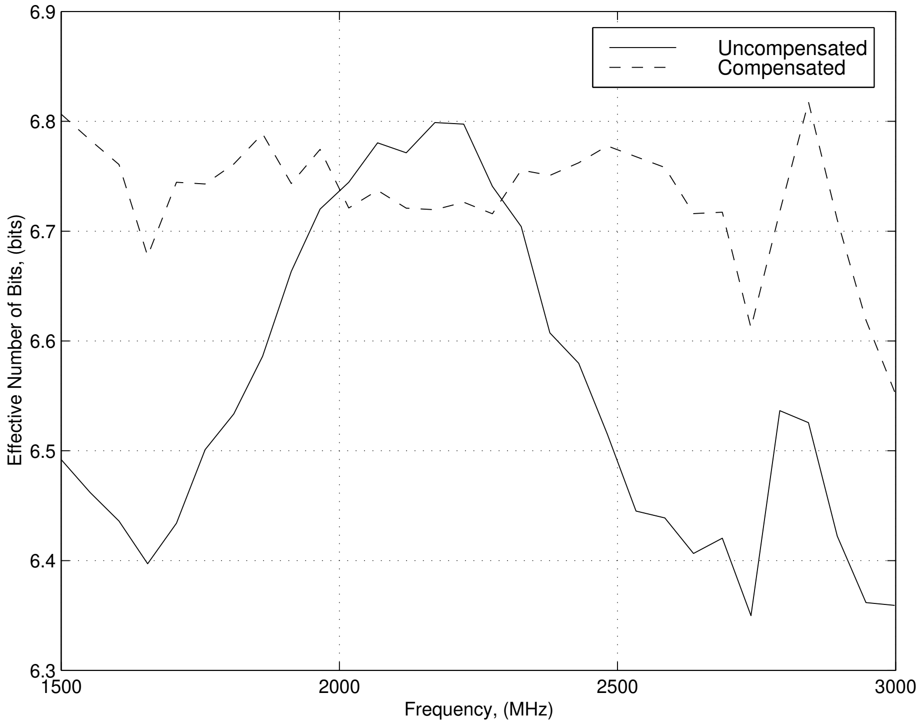

Figure 4.15: Effective Number of Bits over the second Nyquist band, experimental data

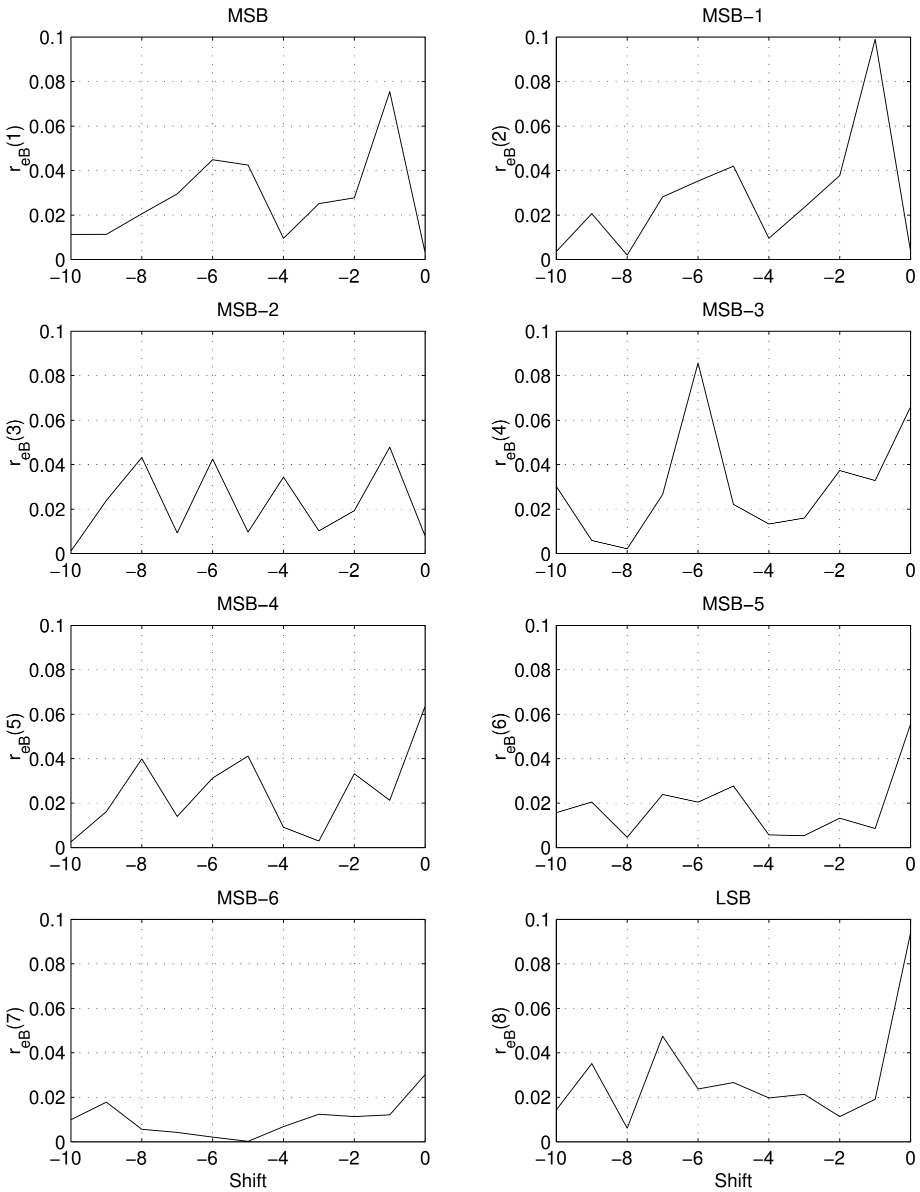

Figure 4.16: Correlation plot after compensation has been performed, experimental data

This compensation routine eliminates all repeatable previous bit dependent error present in an ADC. The results of testing this routine have proven successful and promising. There are several conclusions to be drawn from them, which are discussed in the next, and final chapter.

CHAPTER 5

Conclusions

This thesis has developed shifted-bit error detection and compensation schemes. These tools have proven effective in simulations and on real ADC data. The results are very promising but at the same time demonstrate a need for further investigation. Section 5.1 sums up the results of the shifted-bit correlation techniques.

5.1 Shifted-Bit Correlation Plots

Shifted-bit correlation plots are a useful tool for determining whether or not there is a dependence of ADC error upon previous bits out of a converter.

Figure 4.1 shows correlation coefficients for a simulated ADC with error due to 4 previous bit values. The resulting spectral plots show the error has a significant relation to these shifted-bit values. Figure 4.10 shows similar plots for real data. In these plots at a shift value of zero clock cycles, the error is as strongly correlated as the simulated data, but as the compensated spectral plots show, shifted-bit error is not the sole error mechanism. However, in the majority of the test trajectories this error is dominant (as a third harmonic).

Once the compensation has been completed the correlation plots no longer exhibit strong linear dependence between the error and past bit values as shown in Figures 4.7 and 4.16. In Figure 4.16 the remaining correlation is a little more significant than the theoretical plot because in mid-Nyquist frequencies the routine "over compensates." By over compensating, the routine essentially adds in some previous bit dependence. This shows up as a correlation magnitude of approximately 0.1 in the MSB-1 bit and LSB.

5.2 Previous Bit Dependent Error Modelling

Modelling the error once a linear dependence has been established is relatively easy in concept yet difficult in computational efficiency. A method of estimating the amount of shifted-bit dependent error is presented in summary in Section 3.5. This procedure is based upon the slow orthogonal search which is carefully designed to control the amount of memory used. With an error model created, the ADC under test can then be compensated using the method outlined in Section 3.6. The results of three theoretical and real data sets are shown in Chapter 4.

The theoretical results compensated fully since the only error mechanisms present are shifted-bit errors. The data from the actual converter did not fare as well. The real data is dominated by a shifted-bit dependent third harmonic for both the lower and upper Nyquist frequencies. In the mid-Nyquist frequency this mechanism is no longer dominant. This is clear from the SFDR plot, Figure 4.14. In the mid-Nyquist frequencies the SFDR is not improved by the application of compensation. In fact, the routine actually over-compensates adding a small amount of distortion back into the converter's output. This phenomena is not very easy to explain. The data used were collected at an external site where the conditions for which every set of data collected may not have been the same. Another possible reason for this discrepency may be that in the mid-Nyquist frequencies the dominant error is something other than shifted-bits. In this region of operation the error could be state and slope dependent in which case another compensation technique could be used to enhance improvement. Regardless, the SFDR plot of Figure 4.14 maintains approximately a constant value of 50 dB over the entire second Nyquist band after compensation is employed. Along with this the ENOB has been slightly improved demonstrating that this compensation doesn't add low-level distortion as a consequence of improving SFDR.

Although the results for real converter data are not astounding, at the same time they have proven to be very promising. This source of error has shown to dominate one high-speed converter and could quite possibly appear as a second order source of error in a lower-speed converter. Major contributions from this work have been twofold, namely: it introduces a diagnostic procedure to clearly display the presence of possible shifted-bit dependent errors, and it demonstrates how to compensate for such detected errors with compensation that is simple to implement, is broad band, and does not adversely affect the ENOB measure for the ADC.

REFERENCES

[1] Wahid Ahmed. Fast orthogonal search for training radial basis functions neural networks. Master's thesis, University of Maine, Dept. of Electrical and Computer Eng., Orono Maine, 1994.

[2] S. Chen, C. F. N. Cowan, and P. M. Grant. Orthogonal least squares learning algorithm for radial basis function networks. *IEEE Transactions on Neural Networks*, 1991.

[3] Norm Dutil. Implemetation of dynamic compensation for analog-to-digital converters. Master's thesis, University of Maine, Dept. of Electrical and Computer Eng., Orono Maine, 1997.

[4] R. Gray and T. Stockham Jr. Dithered quantizers. *IEEE Trans. Inform. Theory*, pages 805–812, 1993.

[5] D.M. Hummels, F.H. Irons, R. Cook, and I. Papantonopoulos. Characterization of ADCs using a non-iterative procedure. *Proceedings of IEEE International Symp. on Circuits and Systems*, 1994.

[6] F.H. Irons, D.M. Hummels, and I. N. Papantonopoulos. ADC error diagnosis. In *Proceedings of IEEE International Instrumentation and Measurement Technology Conference*, Brussels, 1996.

[7] M. J. Korenberg and L. D. Paarmann. Orthogonal approaches to time-series analysis and system identification. *IEEE SP Magazine*, 1991.

[8] Jonathan Larrabee. ADC compensation using a sinewave histogram method. Master's thesis, University of Maine, Dept. of Electrical and Computer Eng., Orono Maine, 1997.

[9] James McDonald. Adaptive compensation of analog-to-digital converters. Master's thesis, University of Maine, Dept. of Electrical and Computer Eng., Orono Maine, 1997.

[10] Ioannis Papantonopoulos. Error modelling for folding and interpolating analog-to-digital converters. Master's thesis, University of Maine, Dept. of Electrical and Computer Eng., Orono Maine, 1995.

[11] L. Roberts. Picture coding using pseudo-random noise. *IEEE Trans. Inform. Theory*, pages 145–154, 1962.

[12] L.L. Scharf. *Statistical Signal Processing: Detection, Estimation, and Time Series Analysis*. Addison-Wesley, Reading, Massachusetts, 1991.

Biography of the Author

Eric Swanson was born in Portland, Maine on May 13, 1974. He received his high school education from Gorham High School in 1992.

He entered the University of Maine in 1992 and was selected to be the fifth Castle student in 1994. He obtained his Bachelor of Science degree in Electrical Engineering in 1996.

In May 1996, he was enrolled for graduate study in Electrical Engineering at the University of Maine and served as both a Teaching Assistant and a Research Assistant. His current research interests include communications and signal processing. He is a member of Eta Kappa Nu, and his interests include hiking, camping, and mountain biking. He is a candidate for the Master of Science degree in Electrical Engineering from the University of Maine in May 1998.